Quaternary Science Reviews 172 (2017) 83–95

Contents lists available at ScienceDirect

Quaternary Science Reviews

journal homepage: www.elsevier.com/locate/quascirev

Pleniglacial sedimentation process reconstruction on laminated lacustrine sediments from lava-dammed Paleolake Alf, West Eifel Volcanic Field (Germany)

Luise Eichhorn [a, *], Michael Pirrung [a], Bernd Zolitschka [b], Georg Büchel [a]

[a] Friedrich Schiller University Jena, Institute for Earth Sciences, 07749 Jena, Germany
[b] University of Bremen, Institute of Geography, 28359 Bremen, Germany

ARTICLE INFO

Article history:
Received 12 October 2016
Received in revised form
1 July 2017
Accepted 10 July 2017
Available online 12 August 2017

Keywords:
Lava-dammed lake
Clastic sediments
Lamination
Pleniglacial

ABSTRACT

Differentiating between regularly seasonal, irregular and event-based clastic sedimentation is difficult if sedimentation structures resemble and dating methods are imprecise. In this study - clastic light and dark laminae from lava-dammed Paleolake Alf in the Late Pleistocene in the Quaternary West Eifel Volcanic Field are analyzed to clarify how they formed and if they are of annual origin and comparable to assumed periglacial varves from neighboring Lake Holzmaar. Therefore, a multiproxy approach is applied combining sediment thin section analysis which focuses on composition and structure with ^{14}C dates. The results are compared to recently-formed annually-laminated clastic sediments of, e.g., the High Canadian Arctic. Observed sedimentation structures reveal sediment delivery by over- and interflows and deposition from suspension forming two characteristic microfacies: *Type I* graded laminae and *Type II* laminae with graded sublayers. Additionally, erosional bases and event deposits indicate episodic underflows. Thus, lamination is potentially seasonal but is significantly veiled by extreme runoff causing erosion and resuspension processes or a mixed water body preventing sediment delivery into the lake basin. However, sedimentation processes between watershed and lake could be reconstructed by comparing recent and paleosediment structures.

1. Introduction

Sediments are recorders of past environmental and climatic conditions. Especially clastic laminated lacustrine sediments preserve information about sediment delivery processes generally related to either event-related deposition, e.g., rainfall events or slope instabilities, or to seasonal snow/glacier melt forming annually laminated sediments (varves) (Lamoureux, 2000; Ojala et al., 2012; Zolitschka et al., 2015). Focusing on clastic laminations formed in glacial or periglacial environments, studies in the Canadian High Arctic or Svalbard explain their formation based on monitoring (Cook et al., 2009; Guilizzoni et al., 2006; Leonard, 1997; Zolitschka, 1996). Most abundant particle transport types from the watershed into the lake basin forming a clastic sediment record were considered, e.g., fluvial processes, gelifluction, drifting ice, wave movements and eolian deposition (Retelle and Child, 1996). Menounos and Clague (2008) considered hydrological discharge event monitoring and climate data to differentiate when laminations in the lacustrine sediment were formed. Studies by Francus et al. (2008) focused on temperature and density profiles of the water column to model sediment delivery by over-, inter- or underflows through the lake basin. These observations are especially helpful for the interpretation of sediments, if monitoring data are unavailable, like for paleolakes.

In this study, fluvio-lacustrine sediments from Palaeolake Alf, a volcanically-dammed lake situated in the West Eifel Volcanic Field, are investigated. The lacustrine sediment consists of alternating light and dark laminae which cover the Late Pleistocene immediately prior to the Last Glacial Maximum. As this Paleolake Alf differs from maar lakes due to its elongated shape, a main inlet and a bigger catchment area, it provides an important supplementary archive of this time.

The focus of this study is to give an explanation of the depositional processes that formed the lamination and to examine

* Corresponding author.
E-mail addresses: luise.eichhorn@uni-jena.de (L. Eichhorn), michael.pirrung@uni-jena.de (M. Pirrung), zoli@uni-bremen.de (B. Zolitschka), georg.buechel@uni-jena.de (G. Büchel).

http://dx.doi.org/10.1016/j.quascirev.2017.07.009
0277-3791/

whether the clastic light and dark laminae couplets of Paleolake Alf can be interpreted as varves.

Therefore, the observed laminated sediment structures are compared to modern monitoring studies from glacial or periglacial environments like the Canadian High Arctic or Svalbard (Cook et al., 2009; Guilizzoni et al., 2006; Leonard, 1997; Zolitschka, 1996) to understand related depositional processes.

2. Regional setting

Paleolake Alf is located in the Quaternary West Eifel Volcanic Field. It was formed by volcanic eruptions of the Wartgesberg, their age was determined to 33.6 ± 0.4 ka BP by Schmidt et al. (2017) using luminescence dating, 27.9 ± 2 by Sirocko et al. (2016) using varve chronology, and 31 ± 11 by Mertz et al. (2015) using $^{40}Ar/^{39}Ar$ on groundmass of low-SiO_2 lava.

Lava dammed the formerly V-shaped valley of the River Alf - consequently, the valley was flooded forming an elongated and dendritic lake (Fig. 1) with a reconstructed lake level at 410 m a.s.l.

Paleolake Alf had a watershed of approx. 50 km^2 which was 8 times the size of Lake Meerfelder Maar (Negendank and Zolitschka, 1993), presently the largest maar lake of the WEVF. The watershed of Paleolake Alf consists of peneplains composed of weakly metamorphic clay-, silt- and sandstones of the Siegenian (Saxler Formation) and Emsian stage (Eckfeld Formation) of the Lower Devonian (Meyer, 2013) which were dissected by rivulets and 11 volcanic eruption centers, predominantly maars (Büchel, 1994).

During Marine Isotope Stage (MIS) 3 and 2, Central Europe was

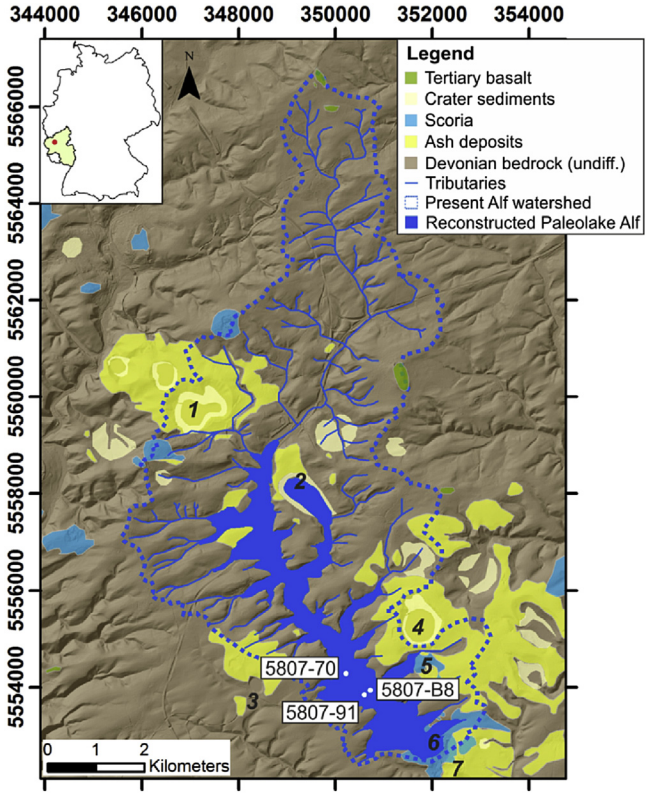

Fig. 1. Study area located in Germany (insert) with the state of Rhineland-Palatinate (in green) and the West Eifel Volcanic Field (red dot). The shaded relief shows the morphology combined with a simplified geology of the watershed of Paleolake Alf, presented in 32 U, WGS84 (Büchel, 1994, State Office for Survey and Geobasis Information Rhineland-Palatinate). Locations of cores 5807-70 (Pirrung et al., 2007), 5807-B8 and 5807-91 are inserted, and young volcanic eruption centers are labelled: ***1***- Dauner Maar complex, ***2*** – Mürmes, ***3***- Holzmaar, ***4***- Pulvermaar, ***5***- Römerberg, ***6***- Wartgesberg, ***7***- Sprinker Maar.

under periglacial conditions. Continuous permafrost dominated with reconstructed temperatures ranging between −20 and + 10 °C (e.g., Huijzer and Vandenberghe, 1998). Arctic steppe tundra with Cyperaceae and *Betula nana* dominated (Litt et al., 2007). During MIS 2, temperatures ranged between −25 and + 11 °C (Huijzer and Vandenberghe, 1998), cold and drier conditions caused loess deposition (Lauer et al., 2014). Debris from physical weathering and solifluction material as well as eolian sediments accumulated on the slopes and in the valleys leading to capacity-limited braided river systems in many areas in Central Europe (Gebhardt, 1963; Houben, 2003; Vandenberghe and Woo, 2002). By the end of MIS 2, snowmelt-driven discharge regimes mostly eroded the periglacial sediments (Gebhardt, 1963; Houben, 2003). Due to the local situation, periglacial erosion did not affect the sediment record of Paleolake Alf and is still preserved – a rare exception in the mountain ranges of Central Europe. Still today, 22 m of rhythmically laminated lacustrine deposits fill the valley bottom under a cover of fluvial sediments.

3. Material and methods

All methods were applied on core 5807-91 (Fig. 2). Different sampling sections derived from differing sediment quality corresponding to the specific method.

3.1. Coring and core handling

During a coring campaign for a hydrological survey in 2012, the 40 m-long sediment core 5807-91 (Latitude = 50° 7.083120′ N, Longitude = 6° 54.598500’ E, WGS84; Z = 32 U, E = 350587, N = 5553848) was recovered from the Alf valley using wireline drilling (diameter: 110 mm). From a preside survey in the Alf valley it is assumed that the coring position is located at the deepest part of the paleolake basin (Fig. 1). After core splitting and lithological description, one half was digitally photographed using the high resolution DMT Core-Scan® from GFZ Potsdam.

3.2. Grain size analysis

Granulometry was determined with a Fritsch analysette 22 on 26 fresh sediment samples. For measurements, 30–60 g of wet sediment was taken between 19.79 and 22.97 m (11 samples from *Unit I*) and laminae-wise between 18.72 and 18.79 m core depth (15 samples of *Unit II*). Samples were mixed with distilled water and sodium pyrophosphate for dispersion. After homogenizing, grains with diameters between 0.31 and 350 μm were analyzed, grains larger than 350 μm did not occur in any of the samples. Prior to each measurement, a purification run including rinsing and ultrasonic was carried out. Grain size distribution data were calculated based on the Fraunhofer optical diffraction model.

3.3. Thin section preparation and microfacies analysis

Between 18.48 and 18.90 m, six large format sediment slabs (10 × 2 cm) with 2 cm overlap were cut from the fresh sediment surface. The samples were shock-frozen with liquid nitrogen for three to five minutes in folded aluminum moulds and freeze-dried for 44 h starting with a temperature of −51 °C. The freeze-dried samples were impregnated with epoxy resin Araldite 2020. A vacuum was applied to extract air bubbles and to allow the resin to penetrate even into the fine pores of the sediment. All further steps concerning cutting, mounting and polishing of the impregnated sediment slab until a sample thickness of 30 μm was achieved were carried out by MKfactory at Potsdam Golm. The final thin sections were sealed by glass cover.

Microfacies analysis was carried out under plain and polarized

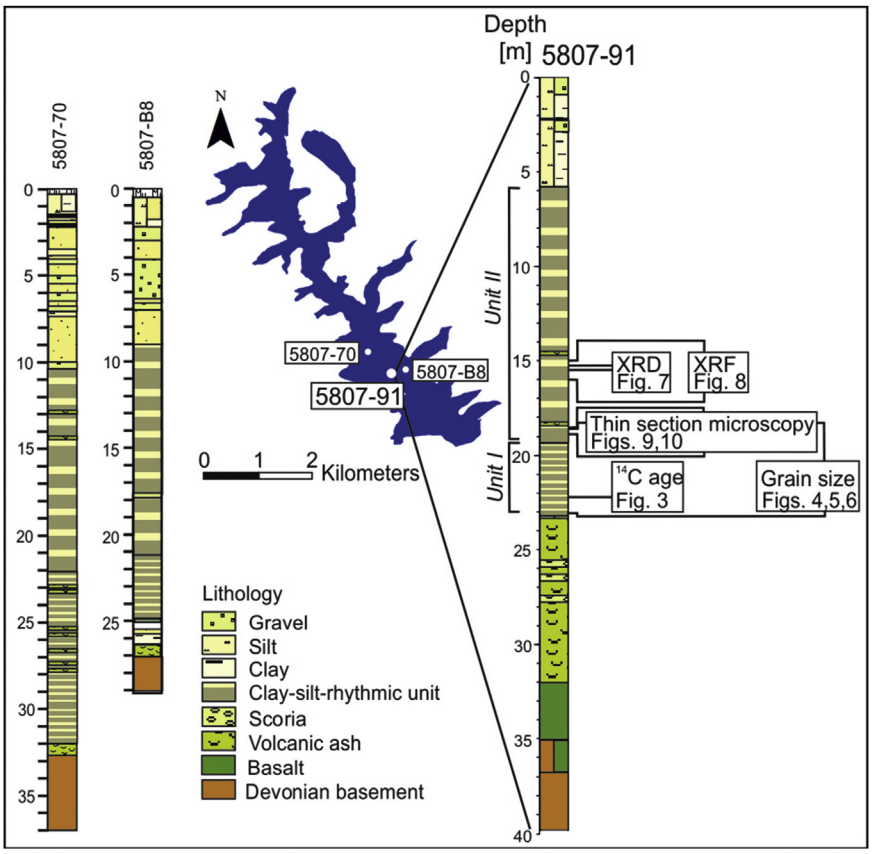

Fig. 2. Location and lithology profile of cores 5807-70, 5807-B8 and 5807-91. Applied methods on core 5807-91 are displayed: X-ray diffraction (XRD), X-ray fluorescence (XRF), grain sizes, thin section microscopy and ^{14}C age.

light with magnifications between 5× and 40 × using a petrographic microscope (Axioplan 2, Carl Zeiss, Jena). Thin section images were taken with a microscope-mounted digital camera (KYF75U, JVC) and the AxioVision (Rel. 4.8) software.

3.4. X-ray fluorescence (XRF)

X-ray fluorescence (XRF) data were obtained using an ITRAX XRF-core-scanner at GEOPOLAR (University of Bremen). Measurements were carried out as a single line scan on a subsampled minicore (U-channel) with the Mo tube at settings of 20 kV, 10 mA and 10 s exposure time. The presented section between 15 and 16 m core depth was analyzed with a resolution of 200 μm. This section was chosen due to its regular laminations without any deformation. Relative element intensities are indicated as counts per second (cps).

3.5. Qualitative mineralogical composition, X-ray diffraction (XRD)

X-ray diffraction (XRD) was examined using a diffractometer (Bruker D8 AXS Advance DaVinci) at Cu Kα radiation (λ = 1.54058 Å). Two samples were analyzed from *Unit II*: one dark (15.37 m) and one light lamina (15.44 m). In *Unit I* the laminae were not thick enough to be subsampled laminae-wise.

The fresh sediment was dispersed with ethanol on a silicon single crystal sample-holder. Diffraction data were collected between 5 and 130 °2θ with a step size of 0.02 °2θ and a dwell time of 10 s. For noise reduction from Fe-fluorescence, the energy window of the detector was set to 0.18–0.25 V. All samples were matched by a full-profile fit with the program DifracEVA® version 4.0 using the database PDF-2 released in 2011.

3.6. Radiocarbon dating

Radiocarbon measurements were carried out via accelerator mass spectrometry (AMS) using the 3 MV Tandetron 4130 AMS at the Leibniz-Laboratory for Radiometric Dating and Isotope Research in Kiel as described by Nadeau et al. (1997). The conventional radiocarbon ages were converted into calibrated calendar years (cal. a BP) by applying the online software CALIB 7.1 (Stuiver and Reimer, 1993) using the IntCal13 calibration dataset, 2 sigma (Reimer et al., 2013). For establishing the age-depth model, a linear interpolation between calibrated means was used.

The age-depth model (Fig. 3) presented in this study is based on one ^{14}C-dating of the humic acid fraction from a bulk sample of core 5807-91 and five AMS ^{14}C determinations from core 5807-B8, situated 175 m east of 5807-91. Another five AMS ^{14}C ages of core 5807-70 (Pirrung et al., 2007), situated 580 m north of core 5807-91 (Fig. 1), were utilized. The dates of both cores were obtained on the humic acid fraction extracted from bulk and wood and projected on core 5807-91 using magnetic susceptibility, lithology and a marker layer. This marker layer is a dark, silty layer and is increased in Si, Ca and most importantly Mn. The latter is most likely deciding for its darkish color. Its thickness measures 0.8 cm.

4. Results

4.1. Mineralogy

The lacustrine sediment of Paleolake Alf mainly consists of

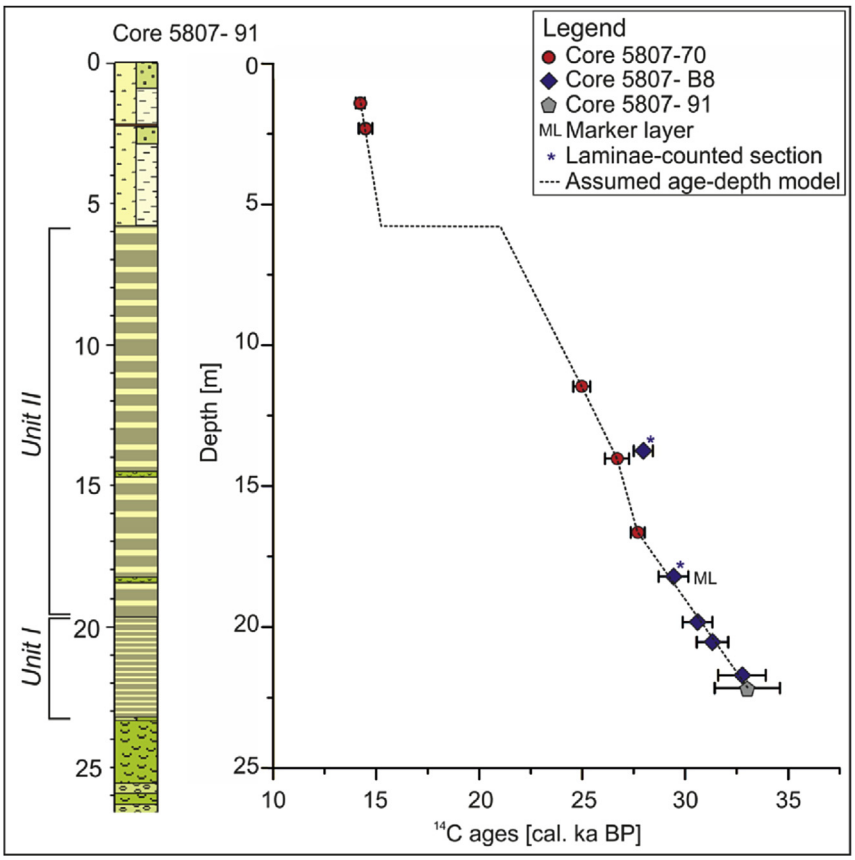

Fig. 3. Age-depth model of core 5807-91. ^{14}C ages of the neighboring cores 5807-70 (Pirrung et al., 2007) and 5807-B8 were projected on core 5807-91 with regards to lithology and a marker. For more details concerning the correlation please see in the Appendix.

quartz, feldspar, transparent mica, chlorite, calcite and opaque oxides. In addition, single idiomorphic, rounded and silt-sized (200 μm) olivine, pyroxene and plagioclase crystals as well as basaltic clasts occur sporadically either isolated or as layers in a fine-grained matrix. Isolated siltstone extraclasts of up to 45 mm were found in the silt-sized sediments, which show hardly any deformation of the underlying sediment. Apart from its mineralogical components, the sediment contains parts of insects, seeds, shell fragments, ostracod valves and pollen (Heike Schneider, 2015, pers. com.).

4.2. Sedimentary units

Core 5807-91 contains Lower Devonian bedrock at its base from 40 to 35 m sediment depth, followed by mafic lava between 35 and 32 m and a mix of scoria and volcanic ashes between 32 and 23 m (Fig. 2). The overlying lacustrine sediments were visually and geochemically separated into *Unit I* (23–19.2 m) and *Unit II* (19.2–5.8 m). *Unit I* differs from *Unit II* due to higher values in potassium in the K/Ti ratio and whereas *Unit II* is characterized by higher Calcium values shown in the Ca/Al and Ca/Ti ratios. The topmost 5.8 m display a mixture of clay- and silt-to gravel-sized sediments interpreted as fluvial deposits (Fig. 2).

Focusing on the laminated lacustrine sequence, *Unit I* is composed of clay-rich silt (on average: 21% clay, 78% silt, 0.08% sand) with a mean grain size of 6 μm. This unit is predominantly characterized by a (sub)millimeter lamination with intercalated slump structures showing a 30 cm-thick folded section with extension faults between 21.00 and 21.30 m, a 45 mm-sized extraclast at 19.75 m and two 30 mm-thick homogeneous sand layers at 20.81 and at 20.97 m depth. Due to the very fine lamination which is partly disturbed, a layer counting of *Unit I* was not possible.

Unit II is composed of light and dark couplets averaging 8 mm in thickness. The light laminae have a mean grain size of 6 μm and are clay-enriched (18% clay, 81% silt, 0.3% sand) whereas dark laminae with a mean grain size of 10 μm contain a higher content of silt particles (9% clay, 90% silt, 0.07% sand, Fig. 4). Within the lamination two volcanic ash layers at 14.56 and 18.31 m are intercalated.

Two graded beds with thicknesses of 4 and 70 mm fining upwards occur with concordant bases from 16.09 to 16.13 m and from 16.65 to 16.72 m. They are interpreted as event-related deposits, i.e. as turbidites. As an example, the grain size distribution of the 70 mm event layer marks a clear fining-upward grain size evolution typical for a turbidite (Fig. 5).

The basal sandy silt layer has a very low clay content and fines upward via a silty central part to a clay-rich top (clay cap) containing highest clay and lowest silt and sand content. Additionally, the grain size distribution shown as cumulative curves reveals the light and dark laminae and the event deposit (Fig. 6).

The curves for dark laminae are shifted by 4 μm towards coarser grain sizes. However, light as well as dark laminae show a similar slope and good sorting, which indicates suspension fall out through a several meter thick water column. The top and middle sections of the event deposit are similarly well-sorted, only the basal layer has a fine tail indicating erosional reworking of the underlying clay layer at the base of the turbidity current. In addition, distal and proximal turbidite sequences of Meerfelder Maar (MFM) are displayed for comparison (Drohmann and Negendank, 1993). The distal turbidite of MFM shows a higher clay content than the light

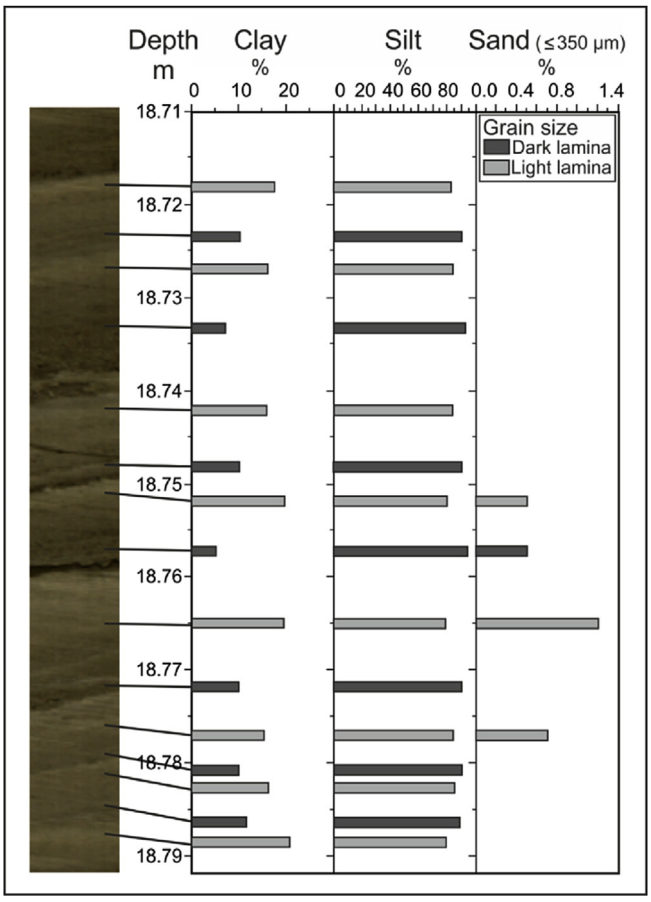

Fig. 4. Grain size distribution presented in volume percent sampled laminae-wise over 71 mm between 18.718 and 18.789 m depth from core 5807-91. Light and dark laminae of *Unit II* are implied by bright and dark gray boxes, respectively.

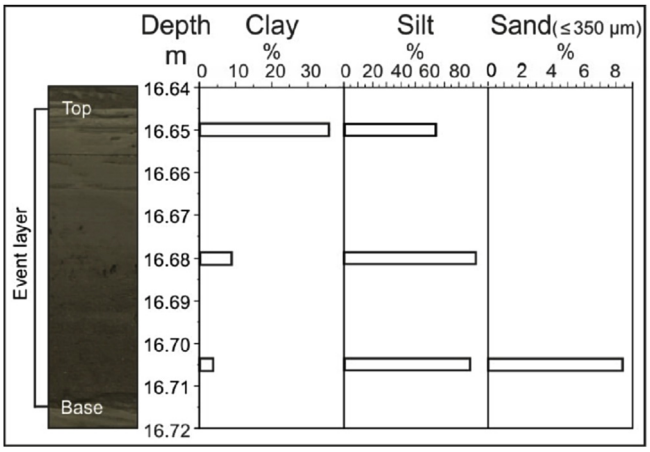

Fig. 5. Grain size distribution presented in volume percent of the 70 mm thick and graded event-layer between 16.645 and 16.715 m depth of core 5807-91.

laminae of Paleolake Alf whereas the proximal turbidite of MFM contains much more sand.

4.3. Mineralogy and geochemistry of light and dark laminae

XRD-data of the light (15.445 m) and dark laminae (15.375 m), taken from *Unit II*, show that the main mineral phases are quartz, muscovite and chlorite as identified by diffraction reflexes (Fig. 7). Although the mineral phases of both laminae are almost identical, their proportions vary: the light lamina is enriched in phyllosilicates, whereas in the dark laminae quartz dominate.

XRF-data from a sediment section of *Unit II* (15.35–15.60 m, Fig. 8) display a higher K/Ti ratio in the light laminae compared to the dark laminae indicating a higher content of mica in the fine-grained light laminae. Ca/Ti ratio is generally higher in the dark laminae (Fig. 8), which points to the presence of calcite. It is microscopically visible but present in too small proportions to be verified with XRD. In the thick dark and light couplet (15.55–15.565 m), a gradation is indicated by arrows, i.e., Ca-enrichment at the base of the dark laminae and K-enrichment towards the clay top.

4.4. Sedimentary microfacies

Microfacies analysis was carried out by microscopic investigation of thin sections from *Unit II*. For *Unit I* this was impossible, because thin sections cracked during drying due to the higher amount of clay. The thickness of the dark and silt-enriched laminae varies between 0.4 and 18.6 mm with a mean of 5.9 mm (n = 74), whereas the thickness of the light and clay-enriched laminae varies between 0.2 and 8.0 mm with a mean of 1.9 mm (n = 78). Deformation of sedimentary structures by bioturbation has not been observed.

The following two microfacies types are differentiated. Both are randomly distributed throughout the investigated section of *Unit II*.

4.4.1. Microfacies type I: lamination with normal grading

Type I (19% occurrence) is characterized by grain-supported coarse-grained basal silt which fines up towards the clay top. The transition from dark to light laminae is gradational indicated by a smoothly rising clay content (Fig. 9, A). The typical dark lamina thickness of this type varies between 0.6 and 14 mm (n = 14).

4.4.2. Microfacies type II: lamination with graded sublayers

Laminae with graded sublayers are more frequent (81% occurrence). The coarse basal layer is characterized by grain-supported silt (20–60 µm). The upper part of the dark laminae is characterized by graded transitions from silt to clay-sized sublayers ranging from two to eleven (Fig. 9, B). This pattern repeats until the upward fining ends in a distinct light lamina. The typical dark lamina thickness varies between 0.4 and 18.6 mm (n = 60).

4.4.3. Clay caps with isolated grains

Often, the lower parts of the clay-enriched light laminae of microfacies types I and II contain dispersed coarser and isolated silt-sized minerals (Fig. 10, A-C). These dispersed coarse silt grains have the grain size of the overlying dark lamina, rarely they are coarser.

The upper part of the light lamina is often undulated, parts of the clay layer are sheared-off or laminae-thickness variations indicate erosional bases of the overlying sediment (Fig. 10, D-F).

4.5. Chronology

Based on a correlation with the two neighboring sediment cores 5807-70 and 5807-B8, an age-depth model for core 5807-91 was established (Fig. 3). By correlating ^{14}C dates (Table 1, Appendix) and lithology of core 5807-B8, *Unit I* of core 5807-91 was dated between 32,995 and 30,558 cal a BP. For the age of *Unit II*, core 5807-91 was correlated with cores 5807-70 (Pirrung et al., 2007) and 5807-B8 using magnetic susceptibility, lithology and a marker layer revealing a time span between 30,558 and 20,837 cal a BP which

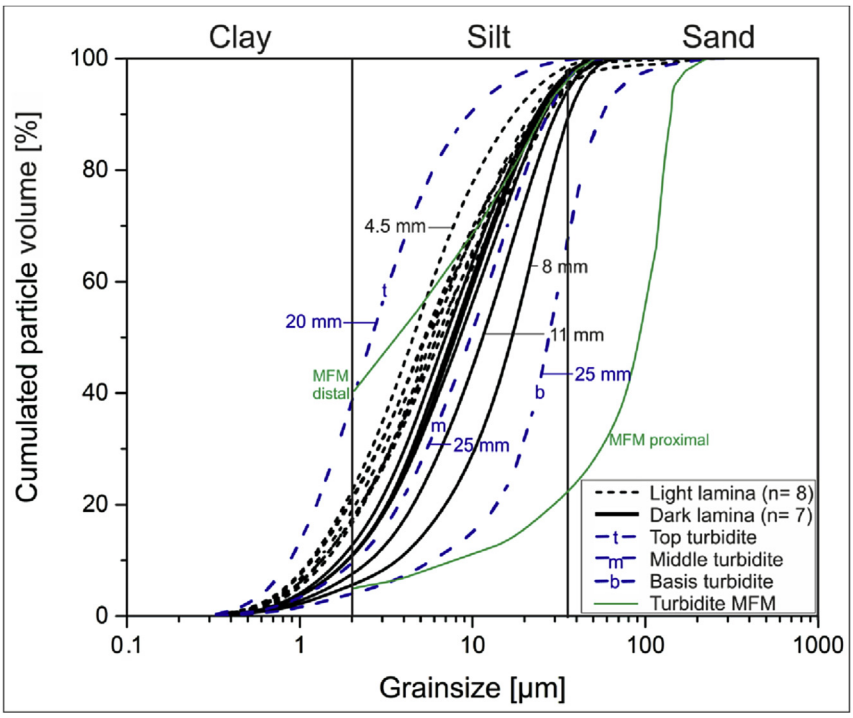

Fig. 6. Cumulative grain size curves showing light and dark laminae (light laminae from core depths 18.718–18.789 m, dark laminae from 18.723 to 18.786 m, cf. Fig. 4) and one event deposit from core 5807-91, cf. Fig. 5. The labels indicating mm reveal layer thicknesses. Green lines show grain size distributions of proximal and distal turbidites from Meerfelder Maar (MFM) for comparison (Drohmann and Negendank, 1993). (For interpretation of the references to colour in this figure legend, the reader is referred to the web version of this article.)

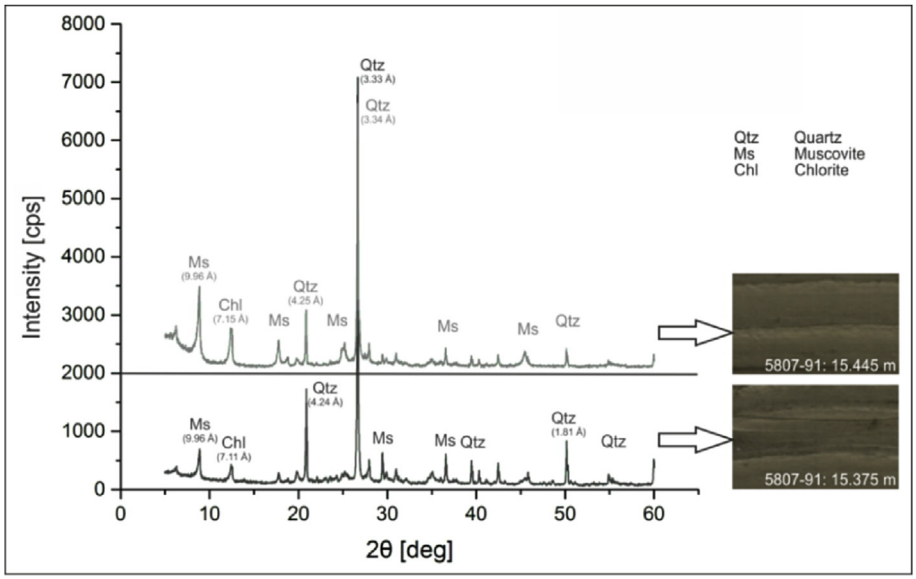

Fig. 7. X-ray diffraction pattern of the light, clay-enriched (top) and the dark lamina (bottom). Their position in the laminated sediments is indicated by the arrow next to the core images. Note that the upper pattern is shifted by an intensity value of 2000 cps for better illustration.

represents approx. 9721 a.

Assuming that one light-dark couplet represents one year, the couplet-counting between 15.35 and 19.90 m depth of core 5807-B8 (projected section marked with a blue star is shown in Fig. 3) revealed 591 couplets, whereas the ^{14}C dates for the same interval covers a time span of 930–1990 a.

5. Discussion

Clastic lamination can be formed by fluvial processes (Retelle and Child, 1996), gelifluction (Doran, 1993), drifting ice (Francus et al., 2008), reworking by waves (Geirsdóttir et al., 2009) and/or eolian input (Antoine et al., 2009). Sediment delivery into Paleolake Alf is supposed to have been dominated by runoff from snow melt

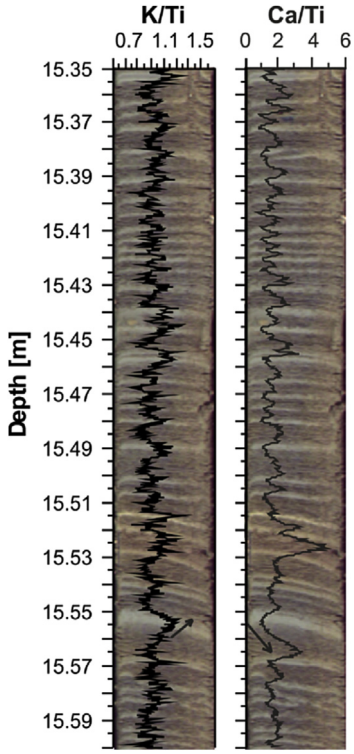

Fig. 8. XRF-data (interpolated 5 point mean) analyzed with 200 μm spatial resolution plotted on the core image demonstrating K-enrichment in the light laminae and a Ca-enrichment in the dark laminae.

and precipitation. The predominant mineral composition of the lacustrine sediments (chlorite, mica, quartz, siltstone extraclasts) resembles that of weathered Lower Devonian bedrock (Felix-Henningsen, 1990) by more than 90%. Sparsely occurring olivines and pyroxenes are typical minerals for basanite volcanism as documented from surrounding maars and scoria cones (Becker, 1977; Shaw and Eyzaguirre, 2000). Certainly, these components entered the lake basin as reworked material. This applies also to the two ash layers which contain mostly subrounded fragments and lack of glass shards (Thor Thordarson, University of Iceland, 2014, pers. com.). Neither in Holzmaar, Meerfelder maar nor Auel maar these two ash layers were described but flood events from that time from Auel maar (Brunck et al., 2016) which supports the assumption that the ash layers were reworked. Single calcite grains of predominantly rounded and the only few calcites of rhombohedral shape implicate a mixture of (1) calcite precipitation in the water column, like they are triggered by algae blooms from recent lakes (Koschel, 1997), and (2) detrital origin as reworked eolian input as documented in a reconstructed high-resolution dust record from Eifel maar lake sediments – the Eifel Laminated Sediment Archive (ELSA) stack (Schaber and Sirocko, 2005; Seelos et al., 2009) and the Holzmaar sediment record (Zolitschka et al., 2000).

The abundance of fine to middle-silt fraction in our laminated sediments can be explained by loess that was found recently at the former crater top of the Wartgesberg quarry. Additionally, the volcanic activity in the watershed of Paleolake Alf provided a high amount of disintegrated bedrock because especially maar eruptions promote up to 90% of country rocks (Zimanowski, 1986).

During the Wartgesberg eruptions, the southern part of the Alf catchment area was covered by ash and scoria. This volcanic ma-

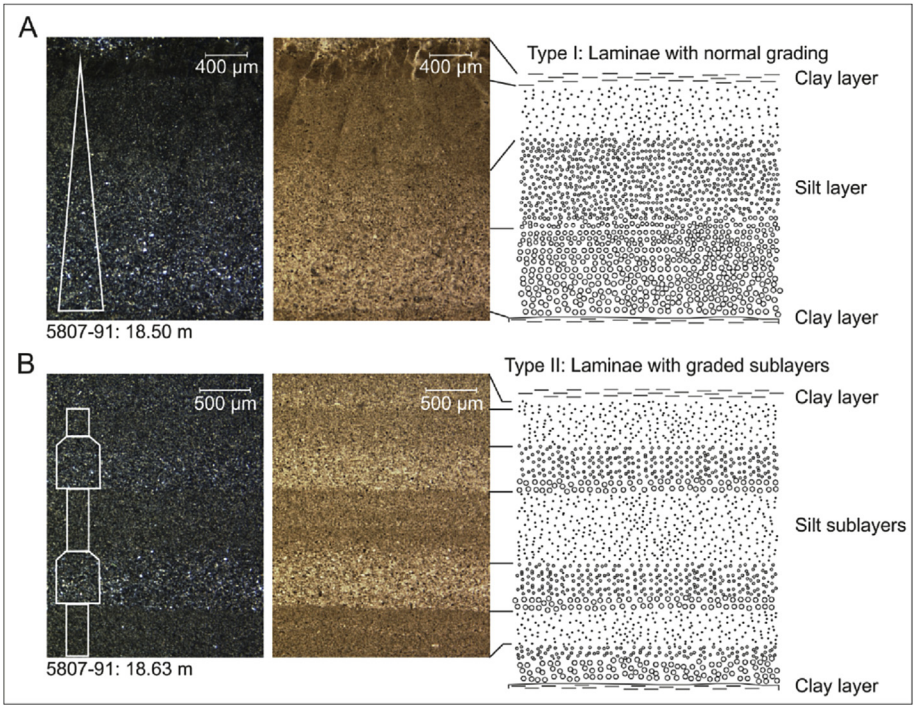

Fig. 9. (A) shows microfacies type I - normal grading of a dark lamina shown under crossed (left) and plain (center) light. (B) shows microfacies type II – laminae with graded sublayers shown under crossed (left) and plain (center) light. A complete lamina of types I and II including the light lamina is also schematically displayed (right). Please note: in contrast to microscopic images, in core scan images the lower coarser part is dark, the upper fine part is light. The core scan nomination is applied throughout the text.

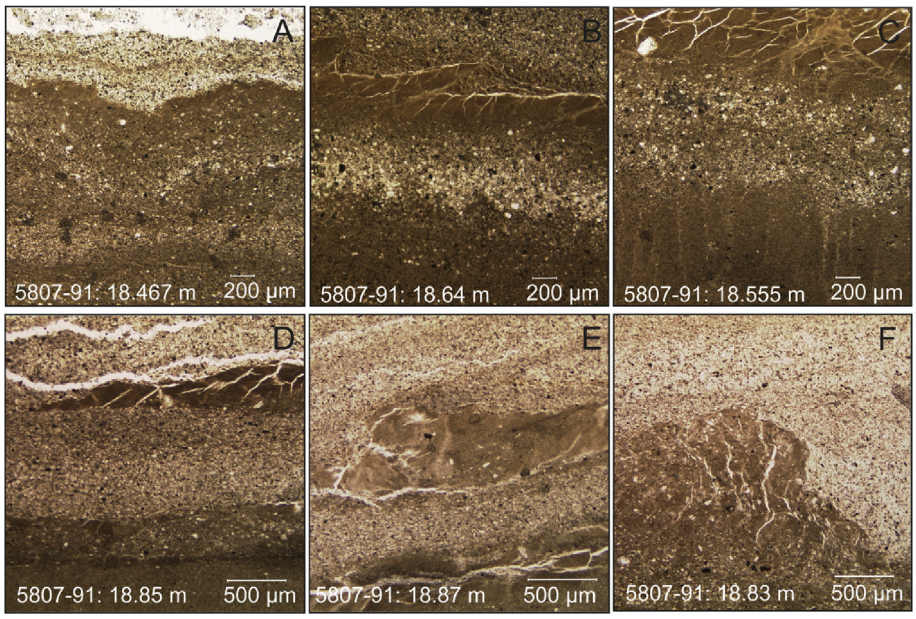

Fig. 10. Microphotographs (plain light) of light laminae with dispersed mineral grains and intercalated silt bands of Type II (A–C). Photos D and E show the transition from light lamina to dark lamina with ripped-off clay fragments embedded in the silty matrix. Clay thickness variations in photo F indicate an erosional base.

terial was eroded and immediately transported into the young lake basin as indicated by the 9 m-thick mix of ashes and scoria on top of the lava flow as documented in core 5807-91. During melting season, catchment sediments were transported to the lake basin: the transport capacity caused a near shore and within-tributary deposition forming subaquatic alluvial fans of coarser sediments near the inlets of rivulets (Fig. 11) whereas silt-sized particles settled from suspension in the center of the lake basin forming *Unit I*.

After the water level reached its final elevation of 410 m a.s.l., Paleolake Alf might also have had a spillover acting like a continuous sediment pull current, probably comparable to observations of the recent spillover at Lehnmühle reservoir (Kämpf et al., 2012).

From correlation of the Paleolake Alf Ca/coh curve (coh stands for coherent radiation which minimizes the matrix effect of the sediment) with the Greenland NGRIP Ca^{2+} curve, *Unit I* formed during Greenland Interstadial 3 (Eichhorn et al., in prep.), Fig. 12.

The higher amount of precipitation during interstadials is reflected in an increased occurrence of slumping indicated by folding structures and event layers in *Unit I*. At around 26,300 ka BP, the amount of calcium increases in both records indicating a cold spell - the Greenland Stadial 3 - with enhanced dust accumulation as described by Schaber and Sirocko (2005) and Seelos et al. (2009), forming *Unit II*. Loess that accumulated on the Devonian ridges was redeposited into the lake basin. The longer onset of the Ca/coh curve in the Paleolake Alf record can be explained with continuing loess cover in the catchment that was longer redeposited. Due to the same mineral composition of the light and dark laminae, the varying silt content can only be associated with seasonal sediment delivery. During the snowmelt season, the high transport energy carried silt-sized, carbonaceous loess that was accumulated in the catchment into the lake basin as indicated by the slightly higher mean grain size of 10 µm and calcite enrichment in the dark laminae.

During winter when the lake is ice-covered, still-water conditions caused suspension settling and the 6 µm-sized particles of the light laminae were deposited. Effectively, grain size and grain shape caused a mineral fractionation in favor of more isometric quartz grains in the dark laminae whereas foliate chlorite and mica grains, due to their higher surface causing uplift, dominate in the light laminae. The 45 mm-sized extraclast and isolated coarse silt grains in the light laminae might indicate a seasonal ice-cover when meltwater slush accumulated on the lake-ice surface as described by Retelle and Child (1996) for Lake C2 in Canada. Load fractures on the ice might have stimulated the meltwater path inducing ice-brake-off. Wind could then have drifted ice floats around the lake in early summer as described by Francus et al. (2008) from Sawtooth Lake in Canada. As documented in core 5807-91, a similar process might have released extraclasts in the center of Paleolake Alf (Fig. 11). Silt bands in the light laminae are interpreted as wind-blown loess deposition on the ice cover.

A further indication for an at least seasonally ice-free lake surface is the abundance of ostracod valves (Fig. 11). They were specified as *Candona neglecta* and *Cytherissa lacustris* (P. Frenzel, University of Jena, pers. com.), interestingly, they were only observed in *Unit II*. *Cytherissa l.* is a glacial species that lives in the littoral and profundal zone of lakes and is not recently living in middle Europe but fossil in shallow glacial and interglacial lake sediments (Fuhrmann, 2012; Meisch, 2000). *Candona n.* is oligothermophil recently occurring in North West Saxony in permanent or slow-flowing water (Fuhrmann, 2012). Both species were also found in the Dehner dry maar in depths between 7 and 34 m (Adams, 2010) equaling a time span between 15,000 and 34,000 a BP (Sirocko et al., 2013).

The question if these laminations are varves, meaning annual deposits (De Geer, 1912), is difficult to answer as processes that drive the formation of theses sedimentary structures are complex. As this clastic lamination is drainage-controlled it depends on whether seasonal discharge took place or not, when and if it appeared once or several times a year. This information is important to ensure a continuous record. Further it is essential to know if the lake waterbody was stratified to transport the sediment suspension along the thermocline into the lake basin or if the lake water was mixed. The two randomly occurring micofacies types forming laminae with normal gradation (*Type I*) and laminae with graded sublayers (*Type II*) suggest single and multiple discharge events under stratified lake conditions. Microfacies *Type I* could have been formed by suspension fall out of an over- or interflow

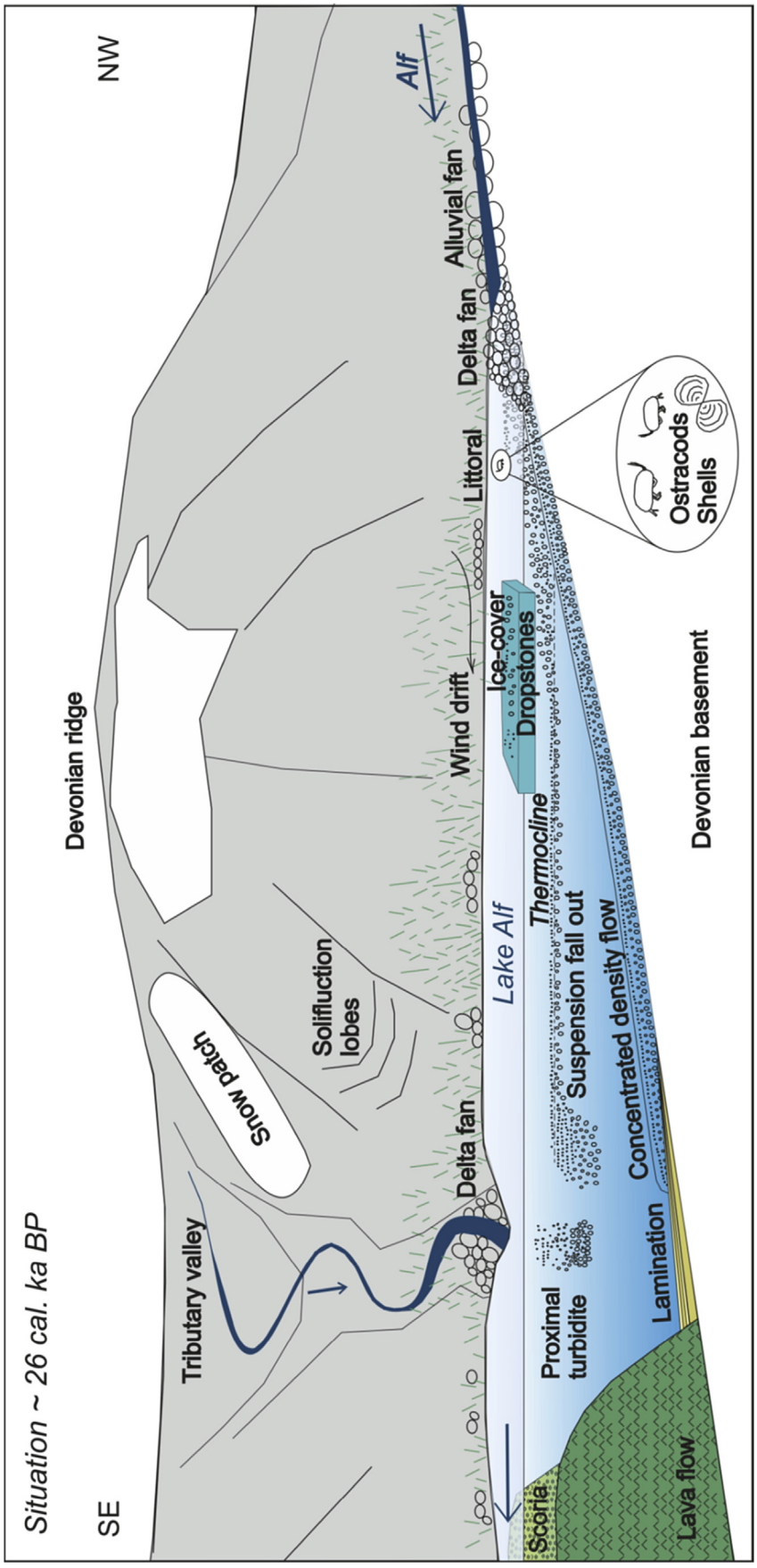

Fig. 11. Sediment structures and components indicating paleoenvironmental processes and conditions are summarized in a conceptual model.

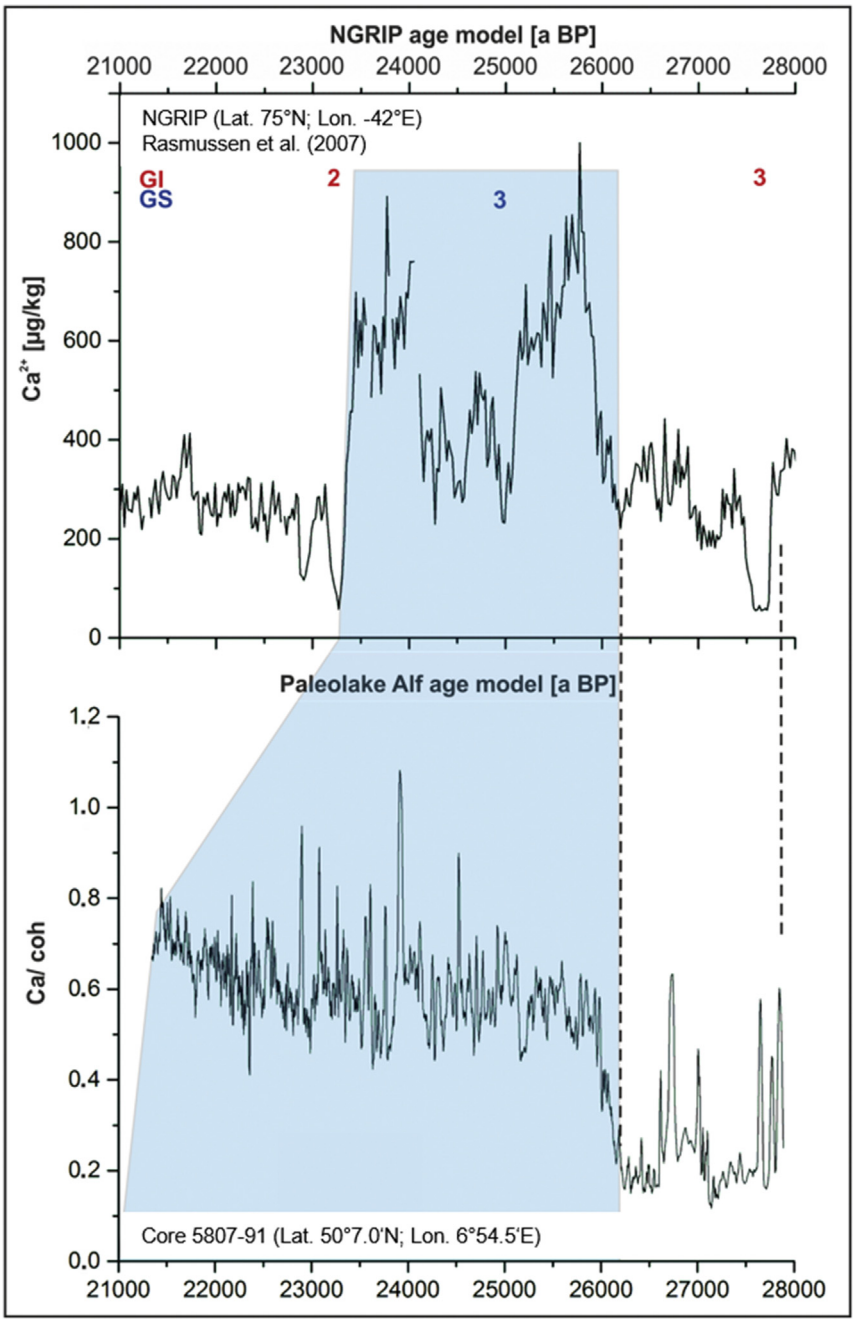

Fig. 12. Correlation of Paleolake Alf with NGRIP ice core using Ca as dust input parameter.

reaching the basin center (Fig. 11). Such conditions are promoted by an early-season discharge when the lake is still stratified due to temperature- and density-differences between the inflowing river and the lake's epilimnion as described by Menounos and Clague (2008) from the Canadian Cheakamus Lake. Microfacies *Type II* suggests repeatedly occurring melting events (between two and eleven; on average six) during summer and/or enhanced precipitation events, as described by Chutko and Lamoureux (2008) for the Canadian Arctic, forming stacked graded sublayers as described by Brauer (1994) for Holzmaar.

The up to several centimeter thick graded beds are interpreted as event-related turbidites in analogy to studies by Mulder and Alexander (2001) that might have formed during mixed lake conditions. These high energy hyperpycnal turbidity currents distribute as concentrated density flows or underflows during the late melt season due to the missing stratification as described by Menounos and Clague (2008) from Cheakamus Lake or if the inflowing river suspension is denser than the lake water. They are triggered by peak water discharge, slope failure or delta front collapse as described by Zolitschka (1996) from Lake C2 on northern Ellesmere Island, Canada. A higher amount of clay in the event layers indicates resuspension of formerly deposited light laminae and a higher amount of sand suggests a more proximal origin of the density current and a higher transport energy, most likely originating from neighboring slopes.

The reconstructed climatic conditions for Central Europe during the Pleniglacial reflect the similar conditions as presently occurring in the Canadian Arctic at, e.g., Iqaliut in Nunavut (WMO ID: 71909,

Canadian Climate Normals, 1981–2010) with cold winters, short summers and prevailing permafrost (Huijzer and Isarin, 1997; Kasse et al., 1998; Vandenberghe and Pissart, 1993) except for, e.g., differing insolation. Therefore, most studies for comparison were chosen from this region. During the short summer period, we assume melting conditions with sediment erosion and transfer. For the other months the environment is under snow and ice cover leading to suspension fallout from the lake water column. Due to the more southern location of Germany and the associated higher solar radiation we suggest that the ice-cover of Paleolake Alf disappeared every summer. Taking these assumptions into account there should be a seasonal signal in the sediments. The regularity and the good sorting of the laminae of Paleolake Alf would support this argument. Also the sedimentation pattern of gradation and stacked graded silt layers are described as probably being related to varves by studies from Holzmaar, Quaternary West Eifel Volcanic Field in Germany (Brauer, 1994) and Lower Murray Lake, High Arctic of Canada (Cook et al., 2009). However, main concerns about an annual mode of deposition are the discrepancy between ^{14}C dating and counted dark-light couplets. An explanation for this could be that not every seasonal sediment delivery has reached the lake basin at the core position so there is a seasonal but irregular deposition. Another possibility might be errors in layers counting as this was only done on high-resolution core scan pictures of 5807-B8 where the ^{14}C measurements were taken from as well. Possibly, the light lamina was eroded in some cases and some sublayers are real varves that we did not identify as such due to their missing clay cap.

Since the time span of ^{14}C ages is two to three times higher than the amount of counted couplets, the ^{14}C dating itself might be questioned because there is hardly any organic matter (humic acid: 1.1–1.5 mg C) preserved for dating under Pleniglacial climate conditions. Another option is resuspension of the rare organic matter either by waves eroding old material from the lake shores as described by Geirsdóttir et al. (2009) from Lake Haukadalsvatn, Iceland, or by density flows incorporating older and already deposited lake sediments.

However, ^{14}C ages of the humic acid fraction show an age of ~30 ka BP for the lowermost lacustrine deposits of Paleolake Alf which is on order of magnitude of what other scientists determined for the Wartgesberg eruption age.

As ^{14}C dating of minerogenic, organic carbon poor sediment is always difficult, the key to a better understanding of the formation of laminae at Paleolake Alf cannot be obtained until further techniques like magneto- and pollenstratigraphy or luminescence dating have been applied successfully in the future.

6. Conclusion

The laminated lacustrine sediments of Paleolake Alf assumedly formed by runoff from snow melt and precipitation predominantly consist of quartz, feldspar, mica, calcite and opaque oxide minerals from frost weathered material of the watershed. Dark laminae formed during summer reflected by higher grain sizes due to higher transport energy, light laminae indicate still water conditions present under ice-cover during winter.

The dominating inner structure of the dark laminae shows graded sublayers (Microfacies *Type II*) suggesting repeatedly occurring melting events during summer and/or enhanced precipitation, less abundant is normal grading (Microfacies *Type II*) which is related to suspension fall out of an over- or interflow.

Due to the regularity of the laminae and seasonal melting, we suggest a seasonal signal in the sediments. However, counted laminae and ^{14}C dates from the same section differ implying partly resuspension.

Acknowledgement

We highly appreciate the support of the engineering company “Wasser und Boden”, Boppard, especially Dr. K.-H. Köppen and the “Kreiswasserwerk” in Cochem-Zell for providing the sediment cores and the State Office for Survey and Geobasis Information Rhineland-Palatinate for providing the digital elevation model of the study area. We thank Dr. P. Frenzel, Dr. M. Wierzbicka-Wieczorek, Dr. R. Bolanz and Dr. T. Voigt from the Institute for Geosciences of the University of Jena for assistance and valuable discussions, Prof. Dr. Á. Geirsdóttir and Prof. Dr. Thordarson from the University of Iceland for valuable discussions and Dr. T. Kasper, Institute of Geography at the University of Jena, for help with thin section preparation. We thank the anonymous reviewers for improving the manuscript with their suggestions. Finally, we thank the project Integrierte Fluiddynamik in Sedimentbecken (INFLUINS) and the GFZ Potsdam for providing the high-resolution core-scan photos. This study was financially supported by the International Max Planck Research School for Global Biogeochemical Cycles, Jena.

Appendix

Table 1
^{14}C ages of humic acid fraction of cores 5807-70 (Pirrung et al., 2007), 5807-B8 and 5807-91.

Core	Sample Name	Original Sample Depth [m]	Humic acid [a BP]	Depth [m] Projected on Core 5807-91	Humic acid [cal. a BP]
5807–70	KIA30251	2.08	12260 ± 50	1.40	14224 ± 50
5807–70	KIA32746	3.01	12400 ± 50	2.30	14486 ± 50
5807–70	KIA32747	12.15	20760 ± 120	11.48	24968 ± 120
5807-B8	KIA50678	15.35	23800 ± 245	13.75	27962 ± 245
5807–70	KIA30254	14.67	22410 ± 260	14.03	26690 ± 260
5807–70	KIA30253	17.27	23530 ± 220	16.65	27690 ± 220
5807-B8	KIA50679	19.90	25260 ± 285	18.21	29422 ± 285
5807-B8	KIA50680	20.90	26630 ± 400	19.82	30591 ± 400
5807-B8	KIA50681	21.80	27230 ± 420	20.53	31318 ± 420
5807-B8	KIA50682	23.80	28870 ± 510	21.71	32748 ± 510
5807–91	KIA50012	22.08	29160 ± 795	22.16	33004 ± 795
5807–70	KIA32748	23.30	25740 ± 325	–	29050
5807–70	KIA30252	25.60	25290 ± 300	–	28500
5807–70	KIA32749	30.25	24690 ± 205	–	27800
5807–70	KIA30255	31.17	24210 ± 300	–	27300

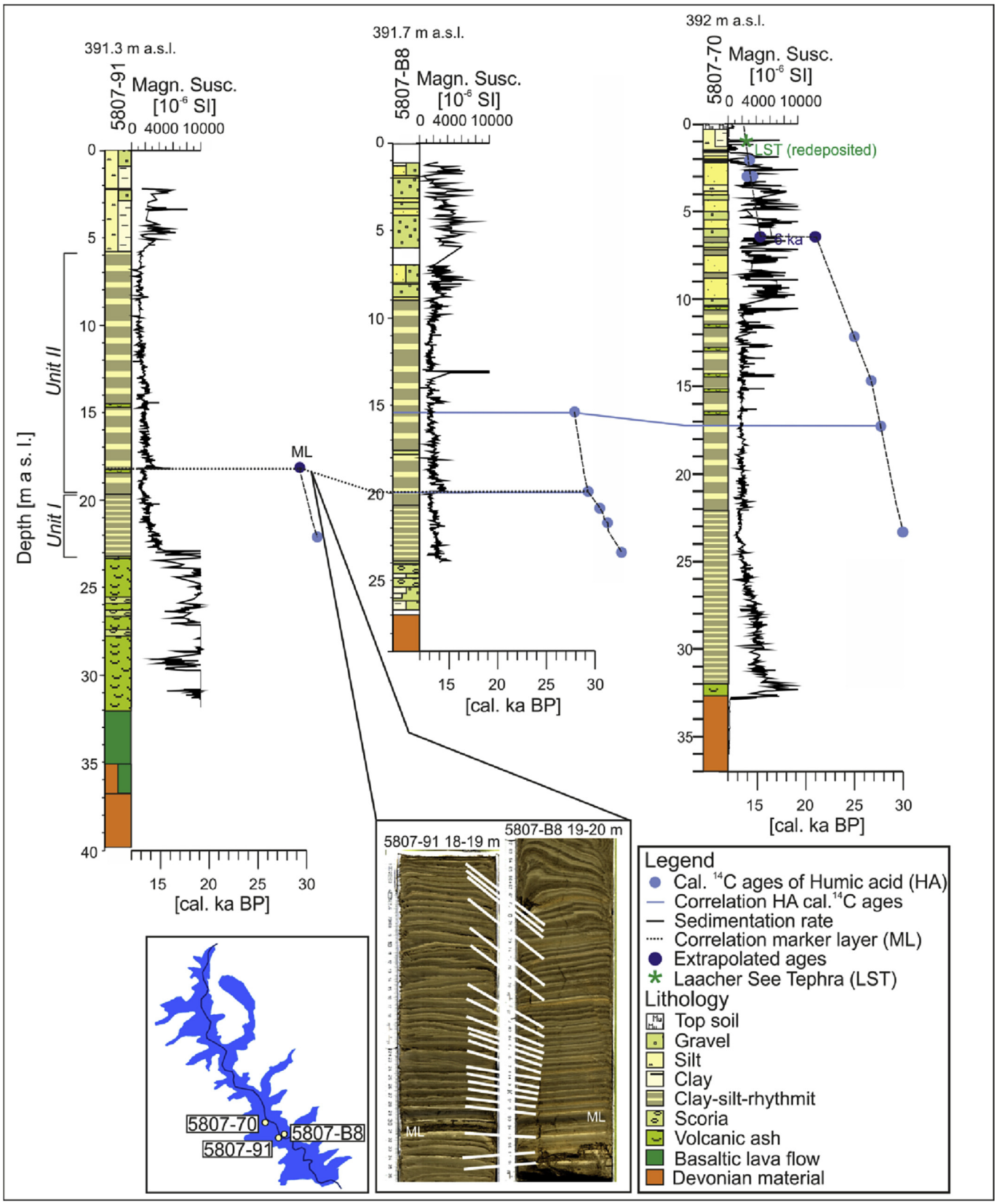

Fig. 13. Core-to-core-correlation using humic acid ^{14}C ages, magnetic susceptibility and a marker layer is displayed. Sedimentation rates of *Units II* and *III* were extrapolated. *Units I* and *II* cover a period between 33 and 21 cal ka BP. Core location (bottom left) and marker layer correlation (bottom middle) is inserted.

References

Adams, C. (2010). Häufigkeit und Isotopensignal von Ostrakoden in Sedimenten aus dem Dehner Maar (Eifel) für die Zeit 13.000–40.000 J.v.h. Diplomarbeit. Johannes Gutenberg-Universität Mainz. (in German).

Antoine, P., Rousseau, D.-D., Moine, O., Kunesch, S., Hatté, C., Lang, A., Tissoux, H., Zöller, L., 2009. Rapid and cyclic aeolian deposition during the Last Glacial in European loess: a high-resolution record from Nussloch. Ger. Quat. Sci. Rev. 28, 2955–2973.

Becker, H.J., 1977. Pyroxenites and hornblendites from the maar-type volcanoes of the Westeifel, Federal Republic of Germany. Contrib. Mineral. Petrol 65 (1), 45–52.

Brauer, A., 1994. Weichselzeitliche Seesedimente des Holzmaars - warvenchronologie des Hochglazials und Nachweis von Klimaschwankungen. Doc. Nat. No. 85, 210 pp. (in German).

Brunck, H., Sirocko, F., Albert, J., 2016. The ELSA-flood-stack: a reconstruction from the laminated sediments of Eifel maar structures during the last 60 000 years. Glob. Planet. Change 142, 136–146.

Büchel, G. (Hrsg.) (1994). Vulkanologische Karte der West- und Hocheifel 1 : 50.000. Landesvermessungsamt Rheinland-Pfalz. Koblenz.

Chutko, K.J., Lamoureux, S.F., 2008. Identification of coherent links between interannual sedimentary structures and daily meteorological observations in Arctic proglacial lacustrine varves: potentials and limitations. Can. J. Earth Sci. 45 (1), 1–13.

Cook, T.L., Bradley, R.S., Stoner, J.S., Francus, P., 2009. Five thousand years of sediment transfer in a high Arctic watershed recorded in annually laminated sediments from Lower Murray Lake, Ellesmere Island, Nunavut, Canada. J. Paleolimnol. 41, 77–94.

De Geer, G., 1912. A geochronology of the last 12,000 years. Compte Rendus XI Sess. Du. Congrés Géologique Int. Stockh. 241–257.

Doran, P.T., 1993. Sedimentology of colour lake, a nonglacial high Arctic lake, Axel Heiberg Island, N.W.T. Can. Arct. Alp. Res. 25, 353–367.

Drohmann, D., Negendank, J.F.W., 1993. Turbidites in the sediments of Lake Meerfelder Maar (Germany) and the explanation of suspension sediments. In: Negendank, J.F., Zolitschka, B. (Eds.), Paleolimnology of European Maar Lakes. Lecture Notes in Earth Sciences, vol. 49, pp. 195–208.

Eichhorn, L., Pirrung, M., Lange, T., Polom, U., Zolitschka, B., Köppen, K.-H., Büchel, G. (in prep.). Basin architecture of lava-dammed Paleolake Alf (Quaternary West Eifel Volcanic Field) compared to modern reservoirs.

Felix-Henningsen, P., 1990. Die mesozoisch-tertiäre Verwitterungsdecke (MTV) im Rheinischen Schiefergebirge: Aufbau, Genese und quartäre Überprägung. Relief Boden Paläoklima. 6. Gebr. Borntraeger, Berlin. Stuttgart, pp. 1–192 (in German).

Francus, P., Bradley, R.S., Lewis, T., Abbott, M., Retelle, M., Stoner, J.S., 2008. Limnological and sedimentary processes at Sawtooth Lake, Canadian High Arctic, and their influence on varve formation. J. Paleolimnol. 40 (3), 963–985.

Fuhrmann, R., 2012. Atlas quartärer und rezenter Ostrakoden Mitteldeutschlands. Altenbg. Naturwiss. Forschungen 15, 1–320 (in German).

Gebhardt, I., 1963. Die Talbildung der Eifel im Ablauf der Klimate, des Vulkanismus und der periglazialen Bodenbildung im Quartär. Dechen 115 (2), 143–214 (in German).

Geirsdóttir, Á., Miller, G.H., Thordarson, T., Ólafsdóttir, K.B., 2009. A 2000 year record of climate variations reconstructed from Haukadalsvatn, West Iceland. J. Paleolimn 41 (1), 95–115.

Guilizzoni, P., Marchetto, A., Lami, A., Brauer, A., Vigliotti, L., Musazzi, S., Langone, L., Manca, M., Lucchini, F., Calanchi, N., Dinelli, E., Mordenti, A., 2006. Records of environmental and climatic changes during the late Holocene from Svalbard: palaeolimnology of Kongressvatnet. J. Paleolimn 36 (4), 325–351.

Houben, P., 2003. Spatio-temporally variable response of fluvial systems to Late Pleistocene climate change: a case study from central Germany. Quat. Sci. Rev. 22 (20), 2125–2140.

Huijzer, A., Isarin, R., 1997. The reconstruction of past climates using multi-proxy evidence: an example of the Weichselian Pleniglacial in Northwest and Central Europe. Quat. Sci. Rev. 16, 513–533.

Huijzer, B., Vandenberghe, J., 1998. Climatic reconstruction of the weichselian Pleniglacial in Northwestern and central Europe. J. Quat. Sci. 13 (5), 391–417.

Kämpf, L., Brauer, A., Dulski, P., Feger, K.-H., Jacob, F., Klemt, E., 2012. Sediment imprint of the severe 2002 summer flood in the Lehnmühle reservoir, Eastern Erzgebirge (Germany). Eiszeitalt. Ggw. – Quat. Sci. 61 (1), 3–15.

Kasse, C., Huijzer, A.S., Krzyszkowski, D., Bohncke, S.J.P., Coope, G.R., 1998. Weichselian Late Pleniglacial and late-glacial depositional environments, coleoptera and periglacial climatic records from Central Poland (Bełchatów). J. Quat. Sci. 13, 455–469.

Koschel, R.H., 1997. Structure and function of pelagic calcite precipitation in lake ecosystems. Verhandlungen Des. Int. Ver. Limnol. 26 (2), 343–349.

Lamoureux, S., 2000. Five centuries of interannual sediment yield and rainfall-induced erosion in the Canadian High Arctic recorded in lacustrine varves. Water Resour. Res. 36 (1), 309–318.

Lauer, T., Von Suchodoletz, H., Vollmann, H., Meszner, S., Frechen, M., Tinapp, C., Goldmann, L., Müller, S., Zielhofer, C., 2014. Landscape aridification in Central Germany during the late weichselian Pleniglacial – results from the Zauschwitz loess site in western Saxony. Z. für Geomorphol. Suppl. Issue 58 (1), 27–50.

Leonard, E.M., 1997. The relationship between glacial activity and sediment production: evidence from a 4450-year varve record of neoglacial sedimentation in Hector Lake, Alberta, Canada. J. Paleolimn 17, 319–330.

Litt, T., Behre, K.-E., Meyer, K.-D., Stephen, H.-J., Wansa, S., 2007. Stratigraphische Begriffe für das Quartär des norddeutschen Vereisungsgebietes. Eiszeitalt. Ggw. Quat. Sci. 56 (1–2), 7–65 (in German).

Meisch, C., 2000. Freshwater Ostracoda of western and central Europe. In: Schwoerbel, J., Zwick, P. (Eds.), Suesswasserfauna Mitteleuropas. Spektrum Akad. Verlag, pp. 1–522.

Menounos, B., Clague, J.J., 2008. Reconstructing hydro-climatic events and glacier fluctuations over the past millennium from annually laminated sediments of Cheakamus Lake, Southern Coast Mountains, British Columbia, Canada. Quat. Sci. Rev. 27, 701–713.

Mertz, D.F., Löhnertz, W., Nomade, S., Pereira, A., Prelevic, D., Renne, P.R., 2015. Temporal-spatial evolution of low-SiO_2 volcanism in the Pleistocene West Eifel volcanic field (West Germany) and relationship to upwelling asthenosphere. J. Geodyn. 88, 59–79.

Meyer, W., 2013. Geologie der Eifel. 4. Aufl. Schweiz.bart. Verlagsbuchhandl, Stuttgart, pp. 1–704 (in German).

Mulder, T., Alexander, J., 2001. The physical character of subaqueous sedimentary density flows and their deposits. Sedimentol 48 (2), 269–299.

Nadeau, M.-J., Schleicher, M., Grootes, P.M., Erlenkeuser, H., Gottdang, A., Mous, D.J.W., Sarntheim, J.M., Willkomm, H., 1997. The Leibniz-Labor AMS facility at the christian-albrechts university, Kiel, Germany. Nucl. Instrum. Methods Phys. Res. Sect. B Beam Interact. Mater. Atoms 123 (1), 22–30.

Negendank, J.F., Zolitschka, B., 1993. Maars and maar lakes of the westeifel volcanic field. In: Negendank, J.F., Zolitschka, B. (Eds.), Paleolimnology of European Maar Lakes. Lecture Notes in Earth Sciences, vol. 49, pp. 61–80.

Ojala, A.E.K., Francus, P., Zolitschka, B., Besonen, M., Lamoureux, S.F., 2012. Characteristics of sedimentary varve chronologies – a review. Quat. Sci. Rev. 43, 45–60.

Pirrung, M., Büchel, G., Köppen, K.-H., 2007. Hochauflösende fluviolakustrine Sedimente des jüngeren Pleistozän aus dem Alfbachtal bei Gillenfeld (Westeifel) - erste Ergebnisse. Mainz. Geowiss. Mitt 35, 51–80 (in German).

Reimer, P.J., Bard, E., Bayliss, A., Beck, J.W., Blackwell, P.G., Ramsey, C.B., Buck, C.E., Cheng, H., Edwards, R.L., Friedrich, M., Grootes, P.M., Guilderson, T.P., Haflidason, H., Hajdas, I., Hatté, C., Heaton, T.J., Hoffmann, D.L., Hogg, A.G., Hughen, K.A., Kaiser, K.F., Kromer, B., Manning, S.W., Niu, M., Reimer, R.W., Richards, D.A., Scott, E.M., Southon, J.R., Staff, R.A., Turney, C.S.M., van der Plicht, J., 2013. IntCal13 and marine13 radiocarbon age calibration curves 0-50,000 years cal BP. Radiocarb 55, 1869–1887.

Retelle, M.J., Child, J.K., 1996. Suspended sediment transport and deposition in a High Arctic meromictic lake. J. Paleolimn 16, 151–167.

Schaber, K., Sirocko, F., 2005. Lithologie und Stratigraphie der spätpleistozänen Trockenmaare der Eifel. Mainz. Geowiss. Mitt 33, 295–340 (in German).

Schmidt, C., Schaarschmidt, M., Kolb, T., Büchel, G., Richter, D., Zöller, L., 2017. Luminescence dating of Late Pleistocene eruptions in the Eifel Volcanic Field, Germany. J. Quat. Sci. 32, 628–638.

Seelos, K., Sirocko, F., Dietrich, S., 2009. A continuous high-resolution dust record for the reconstruction of wind systems in Central Europe (Eifel, Western Germany) over the past 133 ka. Geophys. Res. Lett. 36 (20), 1–6.

Shaw, C.S.J., Eyzaguirre, J., 2000. Origin of megacrysts in the mafic alkaline lavas of the West Eifel Volcanic Field. Ger. Lithos 50, 75–95.

Sirocko, F., Dietrich, S., Veres, D., Grootes, P.M., Schaber-Mohr, K., Seelos, K., Nadeau, M.-J., Kromer, B., Rothacker, L., Röhner, M., Krbetschek, M., Appleby, P., Hambach, U., Rolf, C., Sudo, M., Grim, S., 2013. Multi-proxy dating of Holocene maar lakes and Pleistocene dray maar sediments in the Eifel. Ger. Quat. Sci. Rev. 62, 56–76.

Sirocko, F., Knapp, H., Dreher, F., Förster, M.W., Albert, J., Brunck, H., Veres, D., Dietrich, S., Zech, M., Hambach, U., Röhner, M., Rudert, S., Schwibus, K., Adams, C., Sigl, P., 2016. The ELSA-vegetation-stack: reconstruction of landscape evolution zones (LEZ) from laminated Eifel maar sediments of the last 60,000 years. Glob. Planet. Change 142, 108–135.

Stuiver, M., Reimer, J., 1993. Extended ^{14}C data base and revised CALIB 3.0 ^{14}C age calibration program. Radiocarb 35, 215–230.

Vandenberghe, J., Pissart, A., 1993. Permafrost changes in Europe during the last glacial. Permafr. Periglac. 4, 121–135.

Vandenberghe, J., Woo, M.-k, 2002. Modern and ancient periglacial river types. Prog. Phys. Geogr. 26 (4), 479–506.

Zimanowski, B., 1986. Fragmentationsprozesse beim explosiven Vulkanismus in der Westeifel. Diss. Univ. Mainz, pp. 1–251 (in German).

Zolitschka, B., 1996. Recent sedimentation in a high Arctic lake, northern Ellesmere Island, Canada. J. Paleolimn 16, 169–186.

Zolitschka, B., Brauer, A., Stockhausen, H., Lang, A., Negendank, J.F.W., 2000. Annually dated late Weichselian continental palaeoclimate record from the Eifel. Ger. Geol. 28, 783–786.

Zolitschka, B., Francus, P., Ojala, A.E.K., Schimmelmann, A., 2015. Varves in lake sediments – a review. Quat. Sci. Rev. 117, 1–41.